RSC Advances

ROYAL SOCIETY OF CHEMISTRY

www.rsc.org/advances

Evaluating two new synthesized Schiff bases on the corrosion of copper in NaCl solutions

Yang Zhou†, Shenying Xu†, Lei Guo, Shengtao Zhang*, Hao Lu, Yulong Gong and Fang Gao

Abstract: Two kinds of new Schiff base derivatives, 2-((4-(4-(dimethylamino) styryl) phenylimino) methyl) (DSM) and its intermediate 4-(4-aminostyryl)-N,N-dimethylaniline (AND) form self-assembled monolayers (SAMs) on copper surface. The SAMs have been examined by a series of techniques including contact angle (CA), atomic force microscope (AFM), scanning electronic microscope (SEM), and electrochemical measurements. The results suggest that the two derivatives adsorb on copper surface and generate corresponding hydrophobic films which play an important role in anticorrosion of copper in 3% NaCl solution. Quantum chemical calculations and molecular dynamics (MD) simulation are also used for further insight of the adsorption mechanism.

Key words Electrochemical test, self-assembled monolayer, anticorrosion, Schiff base, copper, theoretical calculations

1. Introduction

Copper and its alloys are extensively investigated and used in industry, owing to high electrical and thermal conductivities as well as excellent mechanical workability.[1, 2] In particular, due to its high strength at low temperature, Cu is used in condenser pipes of ships, coastal power plant heat exchangers and so on. Although its resistance is quite good in nearly neutral or slightly alkaline aqueous environment, copper is still vulnerable to corrosion in harsh condition. As corrosion of Cu in seawater with high concentration of chlorine ions is even more serious, copper anticorrosion in aqueous salt condition is a problem which needs to face up.

There are several methods of copper anticorrosion, *e.g.*, metal coating protective technology (electroplating, chemical, hot dipping)[3], metal surface transformation (metal oxide, metal phosphating, passivation)[4], and non-metallic coating[5]. However, the disadvantages of these approaches, such as low inhibition efficiency, inconvenient operation and environmental pollution, are hard to avoid. Adjusting surface for copper protection with self-assembled monolayers (SAMs) has gained much attention in recent years.[6-8] Thanks to its dense and stable structure, it works as an insulated layer against the penetration of corrosive substances. Up to now, several types of organic compounds have been used for generating SAMs on copper surface for anticorrosion in aggressive environment.[9-11] Generally, compounds having oxygen, nitrogen, sulfur and aromatic rings possess greater stability due to stronger chemical interaction between these atoms and the copper surface.[12]

School of Chemistry and Chemical Engineering, Chongqing University, Chongqing 400044, China.
E-mail:15023289608@163.com; Fax: +86 023 65106756.
† Both authors contributed equally to this work.

Quantum chemical calculations are proved to be a very powerful tool for studying the inhibition mechanism. Adsorption-related electronic properties, adsorption geometries and energies, charge transferred from or toward the surface or a full description of the bonding electronic structure, are useful and can be achieved by means of density functional theory (DFT) methodology.[13-15] Besides, molecular dynamics simulation has also been used to analyze the characteristics of the inhibitor/surface mechanism and to describe the structural nature of the inhibitor in the corrosion process.[16-18] Many results indicated that inhibitor molecules can adsorbe on the copper surface through the π-type bonding of aromatic ring as well as –C=N− double bond. So we inferred if there are more aromatic rings, the strength of adsorption will be stronger. To examine this assumption, AND and DSM were synthesized.

The anticorrosion performances of SAMs formed by AND and DSM have been examined by complementary techniques, such as electrochemical methods, scanning electron microscope (SEM), atomic force microscopy (AFM), contact angle measurement (CAM). Additionally, the relationship between theoretical calculations and experimental results of the SAMs are discussed.

2. Experimental

2.1 Materials and sample preparation

AND and DSM were synthesized in our laboratory. Pure DSM is a yellow and solid and AND is deep yellow. The compounds' synthetic route and molecular structure were presented in Fig. 1. The chemical structures of organic compounds characterize nuclear resonance (NMR) spectroscopy. Tetramethylsilane (TMS) was used as internal standard to determine NMR spectroscopy with Bruker 500 MHz apparatus at the room temperature.

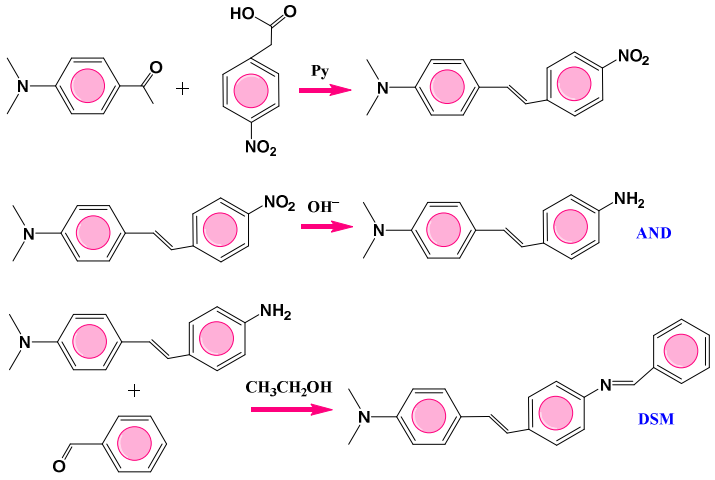

Fig. 1 The synthetic route and molecular structure of AND and DSM.

AND: ^{1}H-NMR (400 MHz, DMSO-d6) δ (ppm): 13.206 (s, 1H, Ar−OH), 8.999 (s, 1H, −N=CH−), 7.629-7.640 (d, J = 4.4 Hz, 1H, Ar−H), 7.600-7.614 (d, J = 5.6 Hz, 2H, Ar−H), 7.405-7.439 (m, 5H, Ar−H),

7.150-7.178 (d, J = 11.2 Hz, 1H, Ar−H), 7.013 (s, 1H, Ar−H), 6.941-6.986 (m, 2H, −CH=CH−), 6.707-7.722 (d, J = 6.0 Hz, 2H, Ar−H), 2.924 (s, 6H, $-N(CH_3)_2$), ^{13}C-NMR (100 MHz, DMSO-d6) δ (ppm): 823.60, 964.41, 1178.51, 1357.89, 1523.76, 1610.56, 3369.94, 3462.22

DSM: ^{1}H-NMR (400 MHz, DMSO-d6) δ (ppm): 7.315-7.330 (d, J = 6.0 Hz, 2H, Ar−H), 7.194-7.208 (d, J = 5.6 Hz, 2H, Ar−H), 6.781 (s, 2H, −CH=CH−), 6.678-6.3993 (d, J = 6.0 Hz, 2H, Ar−H), 6.533-6.647 (d, J = 5.6 Hz, 2H, Ar−H), 2.894 (s, 6H, −N(CH3)2), ^{13}C-NMR (100 MHz, DMSO-d6) δ (ppm): 756.10, 828.53, 947.05, 964.41, 1193.94, 1219.01, 1354.03, 1446.61, 1521.84, 1604.77, 3014.74

2.2. Preparation monolayers on copper

Schiff bases DSM and its intermediate AND were dissolved in tetrahydrofuran in wanted concentration. 3% NaCl solution was prepared as NaCl dissolved in double-distilled water. Pure copper (Cu > 99.5%) was used. Emery papers grading 800 and 1200, 1500, 2000 were used one by one for preparing specimens' surface. And then, the specimens were rinsed by ethanol and immersed into different tetrahydrofuran solutions with different concentrations of DSM or AND for 6 h at room temperature. When the filming process finished, the copper electrodes were taken out from the solution and rinsed by copious quantities of ethanol and double-distilled water.

2.3 Electrochemical tests

All the electrochemical experiments were carried out in a typical three-compartment glass cell, while CHI660B was used. Copper electrodes with and without modified film were used as working electrodes and a platinum electrode as counter one, and a saturated calomel electrode (SCE) as the reference electrode. The reference electrode was connected to a Luggin capillary to minimize IR drop and chloride contamination. All experiments were performed at 298K, using thermostatic Water Bath to keep the temperature constant. The polarization curves were obtained from −250 to +250 mV (versus open circuit potential (OCP)) with 0.1 mV s^{-1} scan rate, and the data were collected and analyzed. Inhibition efficiency was calculated by

$$\eta\% = \frac{I_{\text{corr}}^{0} - I_{\text{corr}}}{I_{\text{corr}}^{0}} \times 100\% \quad (1)$$

where I_{corr}^{0} and I_{corr} indicates the current density in 3% NaCl solution with the bare copper electrode and with the different modified-films-electrodes, respectively.

EIS were carried out at the OCP. The ac frequency range extended from 100 kHz to 10 mHz with a 10 mV peak-to-peak sine wave as the excitation signal. Then the impedance data were analyzed and fitted. The inhibition efficiency obtained from EIS measurements was calculated by

$$\eta\% = \frac{R_{\text{ct}} - R_{\text{ct}}^{0}}{R_{\text{ct}}} \times 100\% \quad (2)$$

where R_{ct}^{0} and R_{ct} are the resistance of charge transfer in the absence and presence of inhibitors.

2.4 Surface Analysis

The morphologies of the copper surface with and without SAMs were examined by SEM and AFM. The SEM and AFM images were taken by KYKY2800B SEM instrument at 25.0 kV and Seiko SPIN 3800N using non-contactmode, respectively. The contact angles (CA) on the bare copper, AND- and DSM-modified copper were measured by sessile water drop method by a contact angle goniometer (Dataphysics OCA20, Germany). The average CA value was obtained by more than five valid measurements on different spots of the same sample.

2.5 Spectroscopic ellipsometry measurement

Spectroscopic ellipsometry is an optical method for surface analysis, which is based on measuring the change of the polarization state of a light beam during reflection.[19] The complex-reflectivity ratio is defined by $\rho = r_\rho/r_s = \tan\psi\exp(j\Delta)$, where r_ρ and r_s are the complex-amplitude reflection coefficients. The angles ψ and Δ are the conventional ellipsometric parameters. The spectroscopic ellipsometry of the thickness of film was measured by M22000U Automatic Ellipsometer (Woollam Corporation, USA). To avoid the strong absorption of light, we selected wavelength range of incident light is 400~800nm with the incident angle of 70°. The optical data was analyzed by the software WVASE32.

2.6 Computational details

All quantum calculations were performed by DFT with Becke's three parameter exchange functional along with the Lee-Yang-Parr nonlocal correlation functional (B3LYP)[20] with the 6-311G++(d,p) basis set as implemented in Gaussian 03.

For an N-electron system with total energy E, qualitative chemical concepts electronegativity (χ) and hardness (ξ) are defined as the following first-order and second-order derivatives,[21]

$$\chi = -\mu = -\left(\frac{\partial E}{\partial N}\right)_{v(r)} \tag{3}$$

$$\xi = \left(\frac{\partial^2 E}{\partial N^2}\right)_{v(r)} \tag{4}$$

where $v(r)$ and μ are the external and electronic chemical potentials, respectively. From the values of the total electronic energy, the ionization potential (I) and electron affinity (A) of the inhibitors are calculated using the following equations,

$$I = E_{(N-1)} - E_N \tag{5}$$

$$A = E_N - E_{(N+1)} \tag{6}$$

where $E_{(N-1)}$, $E_{(N)}$, and $E_{(N+1)}$ are the ground state energies of the system with $N-1$, N, and $N+1$ electrons respectively. And hence χ and ξ are calculated: $\chi=(I+A)/2$, $\xi=(I-A)/2$.

The number of transferred electrons (ΔN) was calculated using the following equation:[22]

$$\Delta N=\frac{\chi_{Cu}-\chi_{inh}}{2\left(\xi_{Cu}+\xi_{inh}\right)}=\frac{\Phi_{Cu}-\chi_{inh}}{2\xi_{inh}} \quad (7)$$

where the work function (Φ) is uesd for the electronegativity of copper surface, and the global hardness is neglected by assuming that for a metallic bulk $I = A$ because they are softer than the neutral metallic atoms.[23]

The adsorption behavior is simulated by Forcite module from Accelrys Inc. The surface Cu(111) was chosen to simulate the adsorption process. The simulation of the interaction was carried out in a simulation box (2.3 × 2.3 × 3.84 nm) with periodic boundary conditions. Cutoff distance was 1.25 nm. Six layers of copper atoms were used to ensure that the depth of the surface was greater than the non-bond cutoff used in calculation. COMPASS forcefield was chosen to optimize the structures of all components of the system. The molecular dynamics simulation was carried out under 298 K, NVT ensemble, with a time step of 1 fs and simulation time of 1000 ps.

3. Results and discussion

3.1 Molecular designs

Schiff bases possess photochemical properties, catalytic activities, structural and electronic properties, ligand effect, and anticorrosion of metals.[24, 25] There are many reports about various Schiff base inhibitors which form complexes with copper ions and generate highly protective films chemisorbing on copper surface.[26-28] The use of nitrogen containing organic compounds as a corrosion inhibitor for copper has been widely investigated. Phenyl rings containing conjugated bonds (π electrons) positively affect the interactions between copper and the inhibitor compound.

We design the new molecule modified with three aromatic rings, and the π-electrons of –C=N–, since molecules containing nitrogen, sulfur, and aromatic rings are known as good corrosion inhibitors for copper in 3% NaCl solution.[12, 29] The SAM formed by DSM is quite stable and it may be attributed to good adsorption of its molecules to the metal surface through interaction within π electrons of the aromatic rings and lone pair electrons of the azomethine (–C=N–) group. Compare to its intermediate (AND), the adsorption mechanism can be better understand.

3.2 Polarization test

The corrosion behavior of copper in NaCl solution has received considerable attention in the literature.[30, 31] Cathodic chemical process occurs as following:

$$O_2 + 4e^- + 2H_2O \rightarrow 4OH^- \quad (8)$$

As contrast, anodic process undergoes a series of complicated and continuous chemical reactions, as demonstrated in Fig. 2. (i) oxidization of Cu(0) to Cu(I), (ii) formation of insoluble CuCl, in presence of anion Cl^-, insoluble film CuCl yields immediately, (iii) formation of soluable cuprous chloride complex, CuCl cannot be fixed due to its weak adhension to copper surface. It is further attacked by Cl^-, and soluble complex $CuCl_2^-$ forms rapidly, (iv) formation of Cu^{2+}, unstable complex diffused from copper surface rapidly undergoes an oxidation reaction, and Cu^{2+} is produced, (V) corrosion of Cu, once Cu^{2+} appears, a disproportionation reaction between Cu(0) and Cu(II) occures: $Cu^{2+} + Cu + 2Cl^- \rightarrow 2CuCl$.

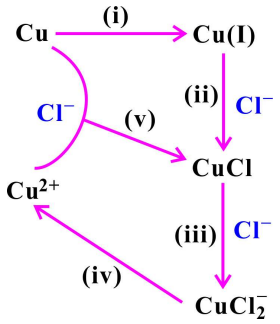

Fig. 2 The corrosion process of copper in 3% NaCl solutions.

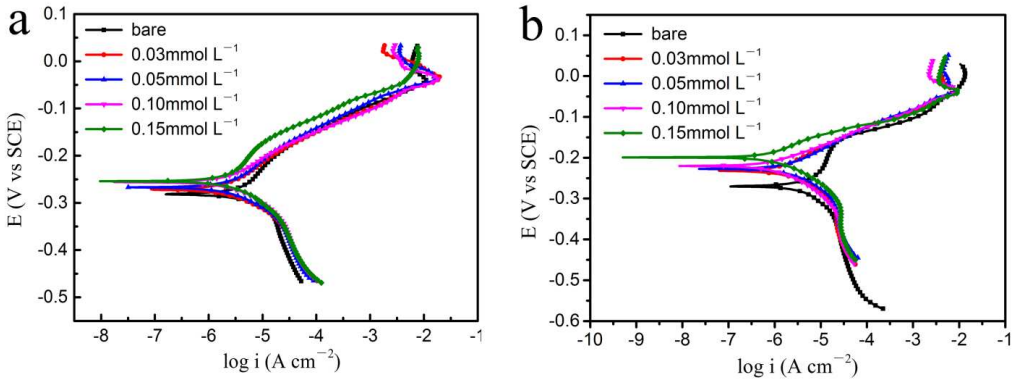

Fig. 3 Potentiodynamic polarization curves obtained in 3% NaCl solution for the bare copper and modified copper electrodes after 6 h of assembly in different concentrations of (a) AND and (b) DSM.

In Fig. 3, both anodic and cathodic reactions of copper electrode were inhibited after modified, and this became more distinct as concentrations increasing. It indicates that after modified AND or DSM reduce copper anodic dissolution and also retards the oxygen reduction. Moreover, the shift in corrosion potential towards more positive value may suggest that the inhibitor molecule mainly functions by inhibiting the anodic dissolution of copper. Moreover, it can be seen from Fig. 3 that the copper electrode displays a Tafel behavior of anodic region. The Tafel line of the anodic polarization curve is extended to the electrode potential below the corrosion potential, and then a vertical line is made parallel to the Y-axis at the corrosion potential. The electrochemical parameters

can be obtained from the point of intersection. In addition, the Tafel slope can be obtained by the Tafel extrapolation method in accordance with the literature[32] as shown in Fig. 4. The corresponding electrochemical kinetic parameters, such as corrosion potential (E_{corr}), anodic Tafel slope (β_a), and corrosion current density (I_{corr}) are listed in Table 1.

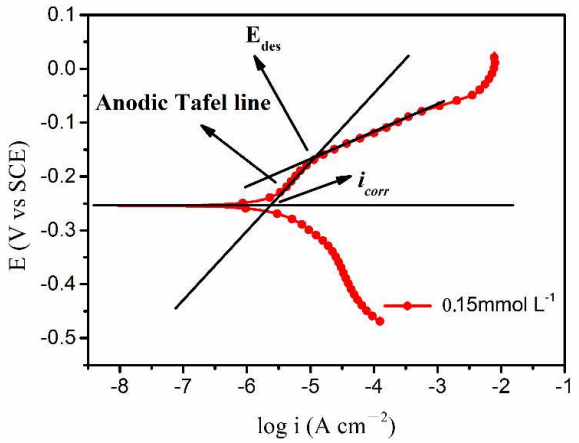

Fig. 4 Tafel extrapolation of the anodic polarization curve for copper with 0.15 mmol L^{-1} AND-modified in 3% NaCl solution.

The effect on β_a values may have many factors, such as the composition of copper electrode, concentration of medium, scan rate, and charge transfer coefficient. Table 1 shows that β_a changes obviously with the modified of AND or DSM, indicating that the adsorbed inhibitor molecules affect mechanism of copper dissolution. Due to the adsorption of AND or DSM on the copper surface, it increases the activation energy of anodic dissolution at the electrode surface. It is observed that the inhibition efficiency increases with increasing concentration. The inhibition efficiency reaches a maximum value (AND: 84.69% at 0.15 mmol L^{-1}, DSM: 94.50% at 0.15 mmol L^{-1}).

Table 1 Polarization curves results obtained in 3% NaCl for the bare copper and the modified copper electrodes after 6 h of assembly in different concentrations of AND and DSM solutions.

	C (mmol L^{-1})	I_{corr} (μA cm^{-2})	E_{corr} (V)	β_a (mV dec^{-1})	SD^a	η (%)
	Bare	10.174	–0.268	500.0	0.01	/
AND	0.03	2.281	–0.272	173.0	0.05	77.58
	0.05	2.149	–0.268	83.3	0.03	78.88
	0.10	1.667	–0.257	62.5	0.05	83.62
	0.15	1.558	-0.256	55.6	0.02	84.69
DSM	0.03	1.170	–0.229	59.0	0.05	88.50
	0.05	1.040	–0.226	41.7	0.03	89.78
	0.10	0.651	–0.219	40.0	0.06	93.59
	0.15	0.559	–0.211	37.8	0.03	94.50

3.3 Electrochemical impedance spectroscopy (EIS)

Figure 5 show the Nyquist plots for the bare copper, AND-modified and DSM-modified copper electrodes after 6h of assembly in different concentrations. From the inset in Fig. 4, the Nyquist plots of the bare copper display a depressed semicircle at the high frequency and follow a straight line at low frequency. The high frequency semicircle may be caused by the charge transfer process, which is related to the relaxation time constant of the charge-transfer resistance (R_{ct}) and the double-layer capacitance (C_{dl}) at the copper/electrolyte interface.[33] The high frequency loop is not perfect semicircles which can be attributed to the frequency dispersion as a result of the roughness and inhomogeneity of electrode surface.[34] The low frequency tail generally is known as Warburg's impedance, which is attributed to the anodic diffusion process of $CuCl_2$ from the surface of the electrode to the bulk solution. And/or to the cathodic diffusion process of dissolved oxygen from the bulk solution to the surface of the electrode. For the AND- and DSM-modified copper electrodes, the Warburg impedance disappears at low frequencies, only some large capacitive loops are observed in Nyquist plots. The disappearance of Warburg impedance indicates that the SAM is sufficiently densely packed to prevent the diffusion process of corrosion reaction and the copper corrosion is controlled by the charge transfer process.

In Fig. 5, several convex arc sexist and each diameter of the arcs increases with the concentration increased. It indicates that the impedance values have increased and the copper has gotten more protection. When the concentration was 0.15 mmol L^{-1}, the capacitive reactance arc radius both reached the largest.

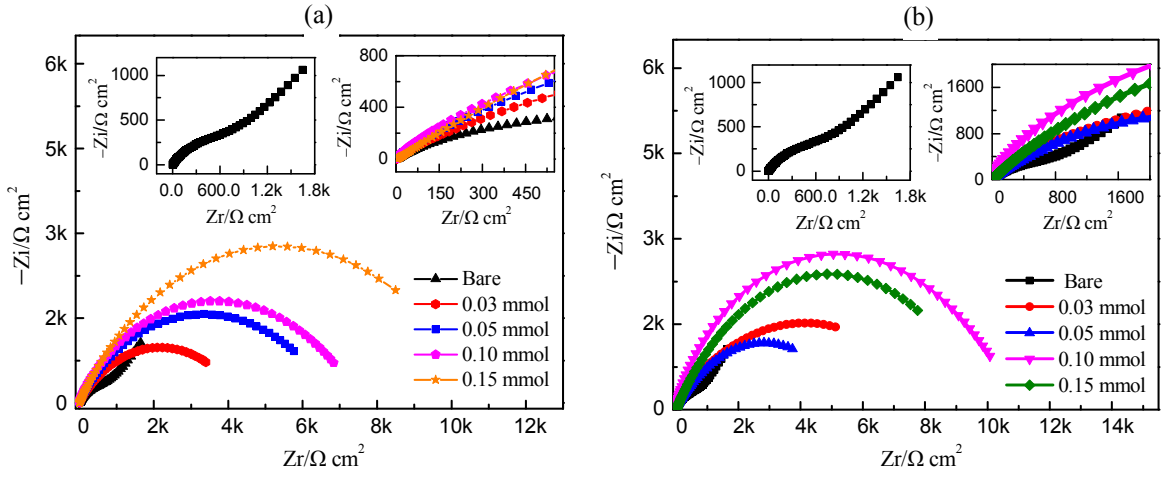

Fig. 5 EIS obtained in 3% NaCl solution for the bare copper and AND-modified (a) and DSM-modified (b) copper electrodes after 6 h of assembly in different concentrations.

The equivalent circuit model employed for this system is shown in Fig. 6. R_s shows the resistance of the solution between the working electrode and the reference electrode. R_{ct} reflects the charge-transfer resistance. R_f is the resistance of the film formed on the copper surface. Constant phase element Q_1 is composed of the membrane capacitance CPE_f and the deviation parameter n_1, and Q_2 is composed of the double-layer capacitance CPE_{dl} and

the deviation parameter n_2.

On the basis of Table 2, the modification of copper increases the R_{ct} values. It seems to be enhanced with the increasing thickness of SAM. η values reach the maximum (AND: 89.20%, DSM: 92.49%) at the concentration of 0.15 mmol L^{-1}. The charge transfer process has been greatly inhibited by SAM, result in preventing copper from corrosion in Cl^- solution. Compared with the blank, the values of corrosive medium increase obviously with AND or DSM concentration in tetrahydrofuran increasing. It suggests that strength of SAM has positive correlation with the concentration of AND or DSM in tetrahydrofuran.

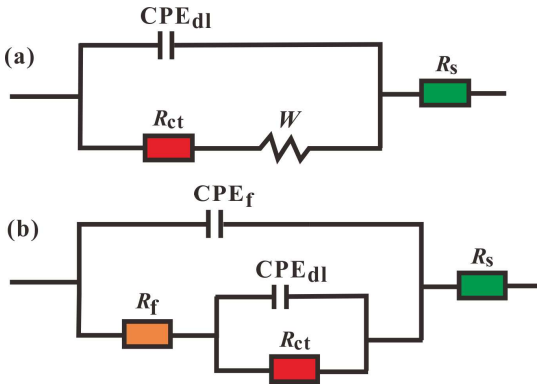

Fig. 6 Equivalent circuit models for the bare copper electrode (a), and the AND- or DSM-modified copper electrode (b) in a 3% NaCl solution.

Table 2 shows that the CPE_{dl} values decrease with the increasing of inhibitor concentrations. Because water molecules are gradually replaced by the adsorption of the inhibitor molecules at metal/solution interface. And it leads to a protective film adsorbing on the copper surface. CPE_{dl} is calculated by equation:[35]

$$C_{dl} = \frac{\varepsilon^0 \varepsilon}{d} S \quad (9)$$

where, ε^0 is the permittivity constant of the air, ε is the local dielectric constant, d is the thickness of the film, S is the surface of the electrode. There may be three reasons that lead to values of CPE_{dl} decrease: the increase in the adsorption film area (which decreases in the electrode surface area), the decrease in the local dielectric constant and/or the increase in the double layer thickness. In a word, the diffusion of ions from the interface to the solution may be delayed and the dissolution reactions of copper may be inhibited to a great extent.

Table 2 Impedance parameters of copper in 3% NaCl solution with different concentrations of AND and DSM.

	C	R_s	Q_f		R_f	Q_{dl}		R_{ct}	W	η
	(mmol L^{-1})	(Ω cm^2)	Y_0 ($\times10^{-5}$ $S s^n$ cm^{-2})	n_1	(Ω cm^2)	Y_0 ($\times10^{-4}$ $S s^n$ cm^{-2})	n_2	(Ω cm^2)		(%)
	Bare					4.253	0.592	938	8.889	/
	0.03	1.616	8.949	1.000	32.69	3.863	0.553	4498		79.14
AND	0.05	1.507	7.571	1.000	33.01	3.679	0.494	5654		83.41
	0.10	1.644	7.368	1.000	34.80	2.556	0.436	7980		88.25

DSM	0.15	1.154	2.209	1.000	35.77	0.395	0.591	8690	89.20
	0.03	1.507	7.571	1.000	33.01	3.680	0.494	5650	83.40
	0.05	1.444	7.968	1.000	34.80	2.515	0.436	8391	88.82
	0.10	3.544	14.05	0.548	37.98	0.488	0.755	9967	90.59
	0.15	3.878	3.634	0.989	39.09	0.151	0.540	11020	92.49

3.4 Contact angle measurements

The wettability of AND and DSM were examined by measuring the contact angle. Fig. 7 shows the images of the sessile water drop on the bare copper, the AND- and DSM-modified copper surface, respectively. It is found that the bare copper has a hydrophilic surface for the contact angle is 72.5° (Fig. 7a), while the angle on the AND-modified copper surface is 93.2° (Fig. 7b) and DSM-modified 102.0° (Fig. 7c). It is evidently seen that the contact angles significantly increase after modification of copper by AND and DSM, indicating of formation of a hydrophobic film. Moreover, the results showed that DSM had better surface hydrophobicity than AND. Generally, the value of contact angle strongly and mainly depends on the structure of adsorption molecule and properties of substrate surface. In the process of adsorption of AND and DSM, the polar head group of these two compounds fix to the copper surface and the nonpolar group is all connecting with solution, resulting in a homogeneous and hydrophobic interface, which gives rise to a larger contact angle.

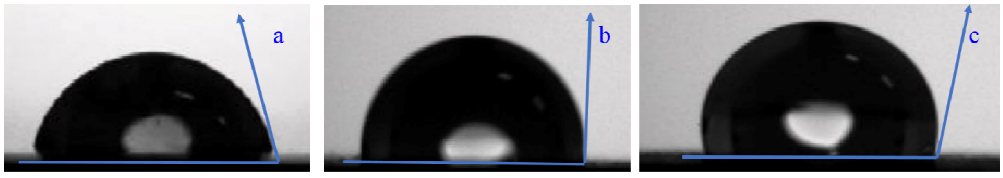

Fig. 7 Sessile water drop images on: (a) a bare copper surface, (b) a copper surface covered with 0.15mmol L^{-1} AND, and (c) a copper surface covered with 0.15mmol L^{-1} DSM.

3.5 SEM and EDS Analysis

Figure 8 shows what happens on bare copper and modified copper electrodes after immersed in 3% NaCl solutions for 3 days. Before corrosion, the surface morphology of the sample was a freshly polished copper surface, as seen in Fig. 8a. After corrosion in 3% NaCl solution for 3 days, the surface morphology becomes porous and rough as shown in Fig. 8b, which means the copper, was severely corroded. Compared with the bare copper, AND-modified copper surface was smooth, but a few middle notches. Moreover, DSM-modified copper was smooth with a few small notches. The fact is indicative of a good inhibition performance of the AND and DSM against copper in 3% NaCl solution.

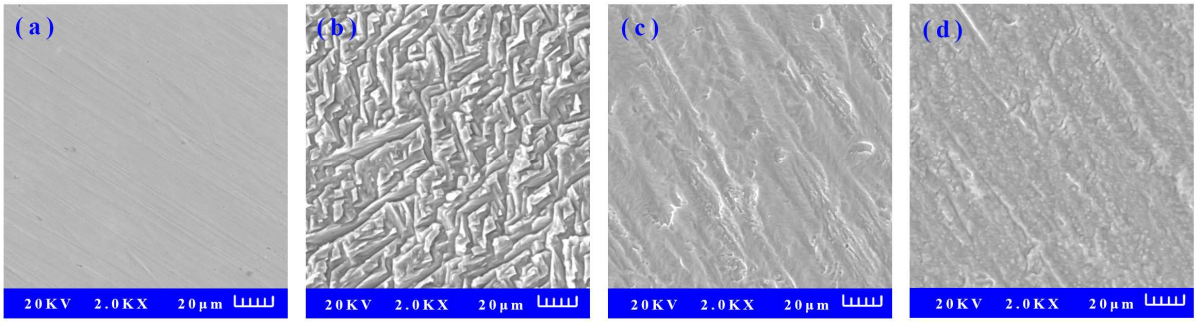

Fig. 8 SEM micrographs of freshly polished copper specimen (a), bare copper (b), 0.15mmol L^{-1} AND-modified (c) and 0.15mmol L^{-1} DSM-modified (d) immersed in 3% NaCl solutions for 3 days.

Figure 9a shows the EDS test results of bare copper. The bare copper mainly consists of copper and a few nickel. However, as shown in Fig. 9b and Fig. 9c, the compositions of surface has changed after the specimen has been immersed in AND or DSM solution. In the images, it can be concluded that the surface is covered by some kind of film, which consists of carbon. However, nitrogen element cannot be observed duo to the high carbon-nitrogen mass ratio (AND: 6.86, DSM: 9.86) and imprecise instrument. Even so, it is fair enough to suggest the formation of the SAMs on the copper surface. It is also shown that the proportion of copper surface is lower than that of AND, meaning the coverage of DSM on copper surface is higher. This conclusion is agreed with results of Electrochemical and SEM tests.

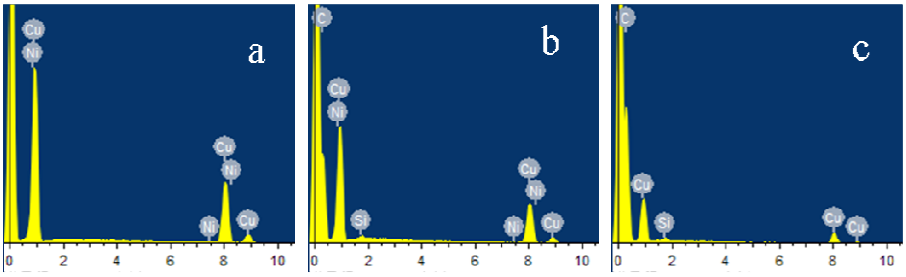

Fig. 9 EDS images of bare copper (a), AND-modified (b), and DSM-modified (c) copper.

3.6 AFM Analysis

The surface topographies of freshly polished copper and modified copper electrodes after 3 h immersed in 3% NaCl solution were shown in Fig. 10. It can be seen that, after modified of AND or DSM, significant differences are found on the surface morphology of the corroded specimens. The AFM image of the freshly polished sample surface looks mostly uniform with only some tiny scratches. When the copper is modified of AND or DSM, the sample surface becomes relatively flat after NaCl treatment in general. And DSM-modified copper surface looks smoother than AND-modified copper surface. The mean roughness of the copper surface before NaCl treatment, after AND and DSA protected treatment are 9.293 nm, 37.60 nm and 12.26 nm, respectively. It suggests that AND and DSM in 3% NaCl solution form a protective film on copper surface which

prevents the surface from corroding.

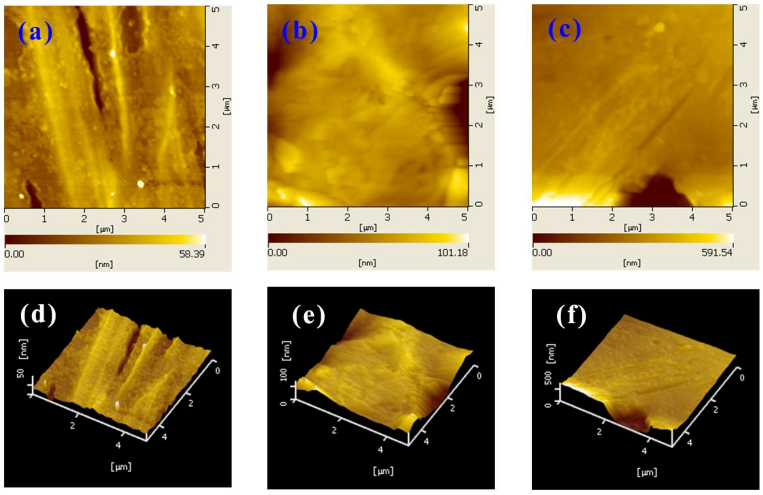

Fig. 10 2D/3D AFM images of freshly polished copper (a,d), AND-modified (b, e) and DSM-modified (c, f) copper immersed in 3% NaCl solutions for 3 h.

3.7 Ellipsometer measurements

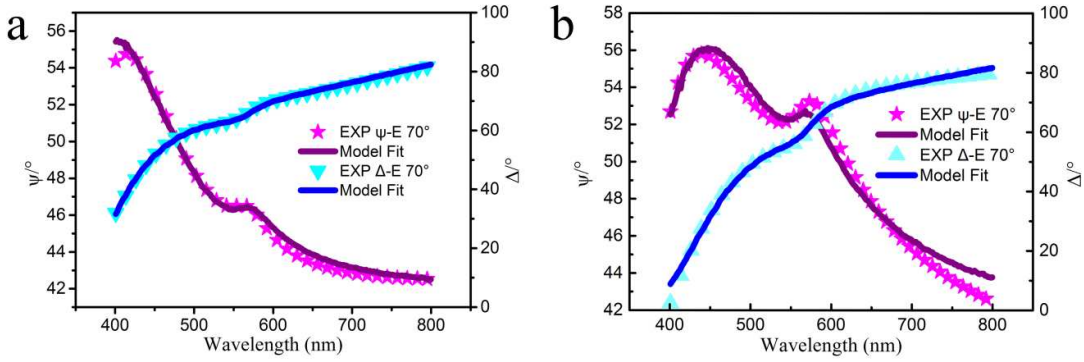

Fig. 11 Fitting results of thickness of AND (a) and DSM (b) modified film

The ellipsometer, a typical tool to test the thickness of the film, was used. Good values are obtained by Cauchy model. The points in Fig. 11 show the results of ψ and Δ of AND- and DSM-modified copper. Because of good permeability of the films between visible spectrum and infrared, the values of thickness of the films have been obtained through Cauchy model[36] (see Fig. 12) by fitting experimental reflectance spectra. The results are presented in Table 3. The values of thickness of film formed in AND and DSM solution are 49.51 nm and 101.56 nm. The larger value, the better anticorrosion ability. So DSM has better performance as it in the other tests.

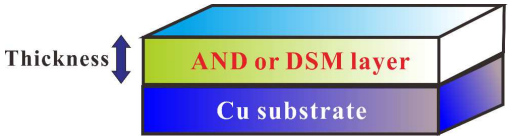

Fig. 12 Cauchy model used for spectroscopic ellipsometry interpretation corresponding to AND or DSM on Cu substrate.

Table 3 Fit results of ψ and Δ by Cauchy model.

	Thickness (nm)	A_n	B_n	C_n
AND	49.5	1.6043	0.00788	−0.0027
DSM	101.6	1.4398	0.08190	−0.0084

3.8 Theoretical calculations

The full optimized minimum energy geometrical configurations of AND and DSM are shown in Fig. 13. The computed molecular properties, including E_{HOMO}, E_{LUMO}, $\Delta E_{LUMO-HOMO}$, dipole moment (μ), surface area (SA), molecular volume (V), projected area (PA), ionization potential (I), electron affinity (A) and fraction of transferred electrons (ΔN), are listed in the Table 4. As seen from the table, the positive ΔN value indicate that the electron transfer from the inhibitor molecule to copper surface is available.

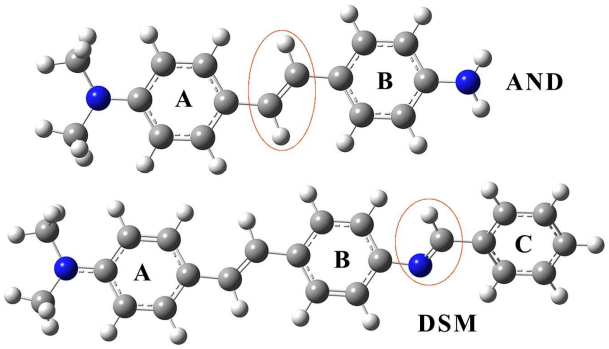

Fig. 13 Optimized structures of AND and DSM

Table 4 Quantum chemical descriptors for the studied inhibitor calculated at B3LYP/6-311G** level.

Inhibitor	μ (Debye)	SA (Å^2)	V (Å^3)	PA (Å^2)	I	A	χ	ξ	ΔN
AND	1.15	309.5	334.42	104.52	4.7	1.09	2.89	1.8	0.53
DSM	3.28	480.11	450.2	131.64	4.98	1.99	3.49	1.5	0.44

In frontier molecular orbital theory, the inhibition efficiency of the inhibitor is closely related to the HOMO and LUMO.[15] It is known that E_{HOMO} is often associated with the electron donating ability of the inhibitor molecule, the higher values of E_{HOMO}, the greater ease of donating electrons to the unoccupied *d* orbital of metal. Whereas, E_{LUMO} indicates the ability of the molecule to accept electrons. So the lower the value of E_{LUMO}, the more probable that the molecule would accept electrons. Thus higher E_{HOMO} and lower E_{LUMO} values generally enhance the inhibition efficiency. Moreover, the smaller value of LUMO−HOMO energy gap (ΔE) for an inhibitor, the higher the inhibition efficiency of that inhibitor.

It could be seen from Fig. 14, the MOs of studied inhibitors are very similar. The MOs, which cover most of the molecular structure, are made up of the π-type bonding in the benzene ring π-bonding and along the −C=N−

double bond (for DSM). This also can be proved by the contribution of some groups to molecular orbitals, which are shown in Table 5. E_{HOMO} of two studied inhibitors are −4.70 eV, −4.98 eV, respectively. The trend of E_{HOMO} is different from the one of efficiency, but difference of two inhibitors is not significant. And the E_{LUMO} are −1.09 eV, −1.99 eV, respectively, so difference of ΔE is huge, 3.60 eV and 2.99 eV, which is identical with the trend of efficiency.

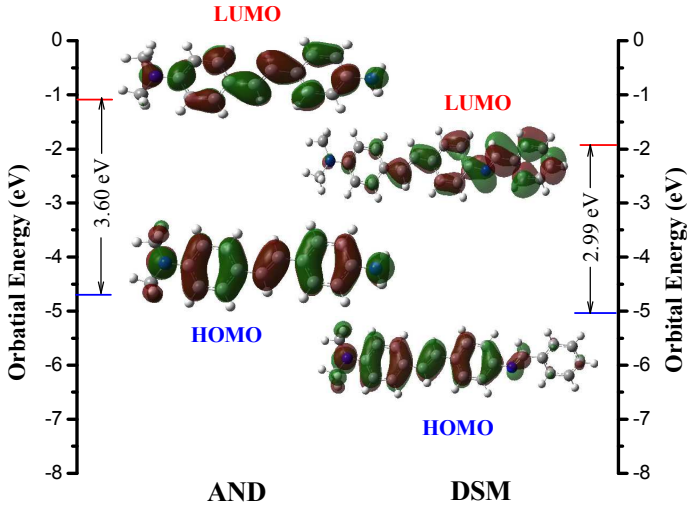

Fig. 14 The frontier molecular orbitals of AND and DSM in HOMO and LUMO

Table 5 Contribution of some groups to the HOMO and LUMO orbitals.

	AND		DSM	
	LUMO	HOMO	LUMO	HOMO
Benzene-A	28.78	31.82	5.78	35.41
Benzene-B	29.91	24.56	19.67	17.30
Benzene-C			31.19	2.34
−C=C−	34.17	21.06	8.95	19.69
−C=N−			32.29	4.51

The total electron density as well as the electrostatic potential (ESP) of AND and DSM are shown in Fig. 15. From an overall perspective, both inhibitors are strong electron donors, for which evidence can be found in the total electron density (Fig. 15a). This has been also confirmed by the electrostatic potential map, in which the negatively charged red regions are located at the upper/lower surface of the molecular skeleton. These electron-rich areas would be preferred sites for adsorption to metal surfaces.

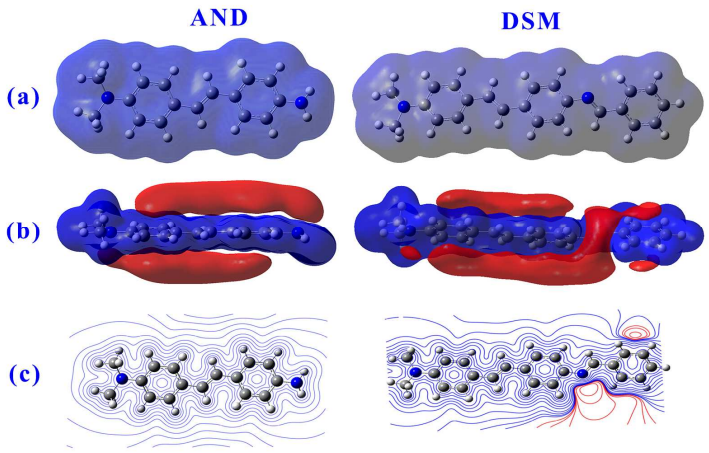

Fig. 15 Electronic properties of the inhibitor molecules: (a) total electron density, (b) isosurface and (c) contour representation of electrostatic potential, respectively. Negative (positive) regions are colored red (blue).

Finally, molecular dynamics simulations were performed to study the adsorption behaviour of specific inhibitor molecules on Cu(111) surface. The close contacts between the inhibitor molecules and copper surface as well as the best adsorption configurations for the compounds were depicted in Fig. 16. It could be noticed that two inhibitors adsorbed nearly parallel to the copper surface through donation of π electrons of the benzene rings and the lone pair of the hetero-atoms to the metal. The average centroid distance (*d*) between inhibitors and the Cu(111) surface is also shown in Fig. 16. The distance of DSM is shorter, this is due to −C=N− double bond and additional benzene ring.

Quantitative appraisal of the interaction was achieved by calculating the adsorption energy (E_{ads}) using Eq. (10):[37]

$$E_{ads} = E_{complex} - \left(E_{Cu} + E_{inh}\right) \quad (10)$$

where $E_{complex}$ is the total energy of the surface and inhibitor, E_{Cu} and E_{inh} is the total energy of the copper crystal and free inhibitor molecule, respectively. The calculated E_{ads} values of the adsorption systems were –332.0 and –438.7 kJ mol^{-1} for AND and DSM, respectively. The larger negative values of interaction energy can be attributed to the strong adsorption between the inhibitor molecules and the copper surface. It is obvious that DSM gives a more negative adsorption energy, which means that adsorption of DSM on Cu(111) surface is more stronger than AND. This accords with their performance in experiments.

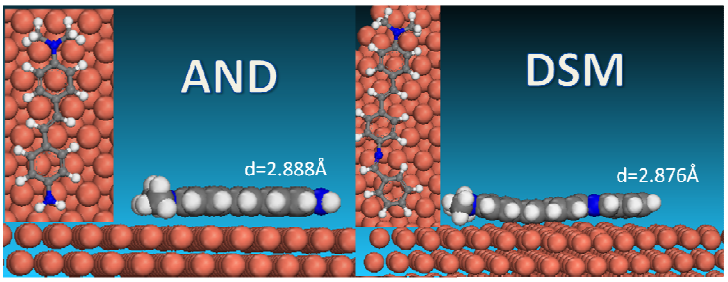

Fig. 16 Representative snapshots of AND and DSM on Cu(111) surface. Inset images show the on-top views.

4. Conclusions

The self-assembled monolayer formed by AND and DSM can protect copper form the corrosion in 3% NaCl solution. The Inhibition efficiency obtained from the polarization text is coincident with ones obtained from EIS, both of them increases with the concentration of impregnation liquid. SAMs formed by AND and DSM on copper surface are characterized by surface analysis. Contact angle, thickness of layers, and corrosion morphology obtained from SEM and AFM indicate that corrosion inhibition efficiency of DSM is better than AND. At the same time, theoretical parameters obtained from DFT calculation and MD simulation, such as energy of the gap, dipole moment, adsorption energy, display the same trend. The results of theoretical calculation are in good agreement with those of experiments.

Acknowledgements

This research was supported by Natural Science Foundation of China (No. 21376282), and Chongqing Innovation Fund for Graduate Students (No. CYB14019).

References

1. R. L. Powell, H. M. Roder and W. J. Hall, *Physical Review*, 1959, **115**, 314-323.
2. A. Bazzaoui, J. I. Martins, E. A. Bazzaoui, L. Martins and E. Machnikova, *Electrochim. Acta*, 2007, **52**, 3568-3581.
3. R. Subasri and T. Shinohara, *Electrochemistry*, 2004, **72**, 880-884.
4. W. H. Leng, D. P. Liu, X. F. Cheng, W. C. Zhu, J. Q. Zhang and C. A. Cao, *Acta Metal. Sin.*, 2007, **43**, 764-768.
5. A. V. Rao, S. S. Latthe, S. A. Mahadik and C. Kappenstein, *Appl. Surf. Sci.*, 2011, **257**, 5772-5776.
6. A. T. Lusk and G. K. Jennings, *Langmuir*, 2001, **17**, 7830-7836.
7. C. X. Li, L. Li and C. Wang, *Electrochim. Acta*, 2014, **115**, 531-536.
8. F. Caprioli, A. Martinelli, D. Gazzoli, V. Di Castro and F. Decker, *J. Phys. Chem. C*, 2012, **116**, 4628-4636.
9. S. M. Song, C. E. Park, H. K. Yun, C. S. Hwang, S. Y. Oh and J. M. Park, *J. Adhes. Sci. Technol.*, 1998, **12**, 541-561.
10. W. Chen, S. Hong, H. Q. Luo and N. B. Li, *J. Mater. Eng. Perform.*, 2014, **23**, 527-537.
11. F. Caprioli, A. Martinelli, V. Di Castro and F. Decker, *J. Electroanal. Chem.*, 2013, **693**, 86-94.
12. M. M. Antonijevic and M. B. Petrovic, *Int. J. Electrochem. Sci.*, 2008, **3**, 1-28.
13. G. Gece, *Corros. Sci.*, 2008, **50**, 2981-2992.
14. L. Guo, W. P. Dong and S. T. Zhang, *RSC Adv.*, 2014, **4**, 41956-41967.
15. I. Lukovits, E. Kalman and F. Zucchi, *Corrosion*, 2001, **57**, 3-8.
16. K. F. Khaled, *J. Solid State Electrochem.*, 2009, **13**, 1743-1756.
17. A. L. Guo, G. C. Duan, K. He, B. Sun, C. C. Fan and S. Q. Hu, *Comput. Theor. Chem.*, 2013, **1015**, 21-26.

18. J. Zhang, G. Qiao, S. Hu, Y. Yan, Z. Ren and L. Yu, *Corros. Sci.*, 2011, **53**, 147-152.
19. G. E. Jellison and F. A. Modine, *Appl. Phys. Lett.*, 1996, **69**, 371-373.
20. A. D. Becke, *J. Chem. Phys.*, 1993, **98**, 5648-5652.
21. S. B. Liu, *Acta Phys. Chim. Sin.*, 2009, **25**, 590-600.
22. R. G. Parr and R. G. Pearson, *J. Am. Chem. Soc.*, 1983, **105**, 7512-7516.
23. A. Kokalj, *Electrochim. Acta*, 2010, **56**, 745-755.
24. R. Noyori and S. Hashiguchi, *Acc. Chem. Res.*, 1997, **30**, 97-102.
25. S. V. Eliseeva and J. C. G. Bunzli, *Chem. Soc. Rev.*, 2010, **39**, 189-227.
26. H. Ma, S. Chen, L. Niu, S. Zhao, S. Li and D. Li, *J. Appl. Electrochem.*, 2002, **32**, 65-72.
27. C. R. Bhattacharjee, G. Das and P. Mondal, *Liq. Cryst.*, 2011, **38**, 441-449.
28. Z. L. Quan, S. H. Chen, L. Li and X. G. Cui, *Corros. Sci.*, 2002, **44**, 703-715.
29. B. E. A. Rani and B. B. J. Basu, *Int. J. Corros.*, 2012, **2012**, 1-15.
30. K. F. Khaled, *Mater. Chem. Phys.*, 2008, **112**, 104-111.
31. A. Dafali, B. Hammouti, R. Touzani, S. Kertit, A. Ramdani and K. El Kacemi, *Anti-Corros. Method. M.*, 2002, **49**, 96-104.
32. M. A. Amin, S. S. A. El Rehim and H. T. M. Abdel-Fatah, *Corros. Sci.*, 2009, **51**, 882-894.
33. J. M. Steigerwald, S. P. Murarka, R. J. Gutmann and D. J. Duquette, *Mater. Chem. Phys.*, 1995, **41**, 217-228.
34. Q. Qu, L. Li, S. Jiang, W. Bai and Z. T. Ding, *J. Appl. Electrochem.*, 2009, **39**, 569-576.
35. S. John and A. Joseph, *RSC Adv.*, 2012, **2**, 9944-9951.
36. M. Rebien, W. Henrion, M. Hong, J. P. Mannaerts and M. Fleischer, *Appl. Phys. Lett.*, 2002, **81**, 250-252.
37. E. E. Oguzie, Y. Li, S. G. Wang and F. Wang, *RSC Adv.*, 2011, **1**, 866-873.